Dynamical Instabilities of Ice X

Razvan Caracas*

Ecole Normale Superieure de Lyon, Laboratoire de Sciences de la Terre CNRS UMR5570, 46 allee d'Italie Lyon, France

(Received 25 April 2008; published 18 August 2008)

Water ice X is stable in the 120–400 GPa pressure range, as obtained from lattice dynamical calculations performed using the density-functional theory. Below 120 GPa, it is characterized by one unstable flat phonon band, which generates the disordered ice X structure. Above 400 GPa, ice X has an unstable phonon mode in M, which leads to the $Pbcm$ orthorhombic structure obtained in previous molecular-dynamics calculations [M. Benoit, M. Bernasconi, P. Focher, and M. Parrinello, Phys. Rev. Lett. **76**, 2934 (1996)]. Therefore, based on lattice dynamics, we propose that the high-pressure low-temperature phase-transition sequence in H_2O ice is ice VIII–disordered ice X–ordered ice X–ice $Pbcm$.

DOI: 10.1103/PhysRevLett.101.085502 PACS numbers: 61.50.Ks, 62.50.−p, 63.20.D−, 64.70.kt

Water is one of the most abundant molecules in the Earth and in the outer solar system. Understanding the behavior of water over a broad range of thermodynamic conditions is of great importance to both Earth and planetary sciences and to fundamental physics and chemistry. In its solid form, water ice forms polar caps and is a major constituents of the plethora of icy bodies present in the outer solar systems or of the solid cores of the giant planets. It is then obvious that building an accurate phase diagram was a scientific priority ever since the beginnings of the high-pressure investigations. Fifteen different crystalline structures have been determined and confirmed experimentally up to date with a few more metastable, amorphous, or modulated structures obtained during different experiments or theoretical investigations [1,2]. It is now accepted that up to about 50 GPa, the sequence of phase transitions in ice consists of a succession of structures in which the molecular integrity is preserved. Above about 50 GPa, the water molecules dissociate [3–5], and in the resulting structure, ice X, the hydrogen atoms lie in the middle between two oxygen atoms, hence the symmetric hydrogen bond ice denomination [3,4,6–8]. The resulting atomic arrangement is ionic, and it represents a characteristic for hydrogen-bearing systems in general at pressures high enough to promote molecular dissociation [9].

The largest pressure-temperature phase space is occupied by the high-density phases VII, VIII, and X [10]. Ices VII and VIII are related by an order-disorder transition—at low temperature in ice VIII, the protons are locked into two of the four half-occupied positions in ice VII. There is x-ray [11], infrared [12,13], and Raman [14] spectroscopic evidence that the transitions between ice VII and X and ice VIII and X are not abrupt but pass through an intermediate disordered structure. The transition sequence has been modeled using first-principles molecular dynamics [7,15] where a similar pattern of atomic displacements as observed in experiments is obtained at finite temperature calculations.

Here, we adopt a different approach and investigate the dynamical stability of ice X using lattice dynamics. We perform first-principles calculations using the density functional theory (DFT) in the ABINIT package implementation [16] based on planewaves and pseudopotentials. We use Troullier-Martins-type pseudopotentials [17] with 40 hartree (1 hartree = 27.2116 eV) kinetic energy cutoff and a $8 \times 8 \times 8$ grid of $\mathbf{k}$ points [18]. These parameters ensure an accuracy of the calculations better than 1 GPa in pressure and 1 mhartree in energy. We use the density functional perturbation theory (DFPT) [19–22] to determine the dielectric tensors, the dynamical charges, and the dynamical matrices. We compute the dynamical matrices on a regular grid of $\mathbf{q}$ points and then apply a Fourier interpolation scheme [20] to obtain the dynamical matrices in any general point of the reciprocal space. We compute the Raman spectra with both peak position and intensity for crystalline powders, using DFPT [23] and an integration formalism described in detail elsewhere [24–27]. We use the Perdew-Burke-Ernzerhof generalized-gradient approximation (GGA) [28] for the exchange-correlation part for all calculations except for the determination of the Raman spectra, for which we use standard Local Density Approximation (LDA).

Ice X has a cubic structure with $Pn\bar{3}m$ space group and two molecules in the unit cell. The O atoms lay in $2a(0\,0\,0)$ Wyckhoff positions, and the H atoms in the $4b(\frac{1}{4}\ \frac{1}{4}\ \frac{1}{4})$ Wyckoff positions, such as each hydrogen atom lays at equal distance to its two oxygen neighbors. Ice X is undistinguishable in x-rays from ice VII. A third-order Birch-Murnagham equation of state fitted on the P-V data yields $V_0 = 25.06$ Å^3, or $a_0 = 2.926$ Å, $K_0 = 198$ GPa, and $K' = 3.73$.

Figure 1(a) shows the phonon band dispersion at 160 GPa. At this pressure, well inside the experimental stability field of ice X all the phonon modes have positive frequencies, confirming the dynamical stability of the structure at these conditions. The phonon bands are highly dispersive. Because of the molecular dissociation, there is no high-frequency hydroxyl flat band characteristic to other H-bearing systems at low pressures.

Under decompression, the structure shows a softening of one phonon mode [Fig. 1(b)]. This mode flattens and soft-

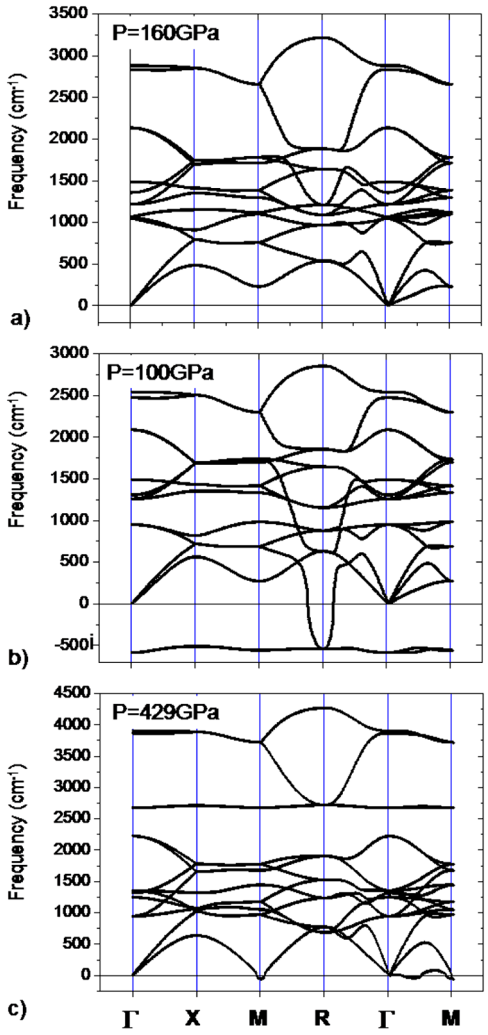

FIG. 1 (color online). Dispersion of the phonon band of ice X at several pressures. The structure is stable in the 120–400 GPa pressure range (a). Below this pressure, it exhibits a flat unstable phonon mode (b) and above an unstable phonon in M (c).

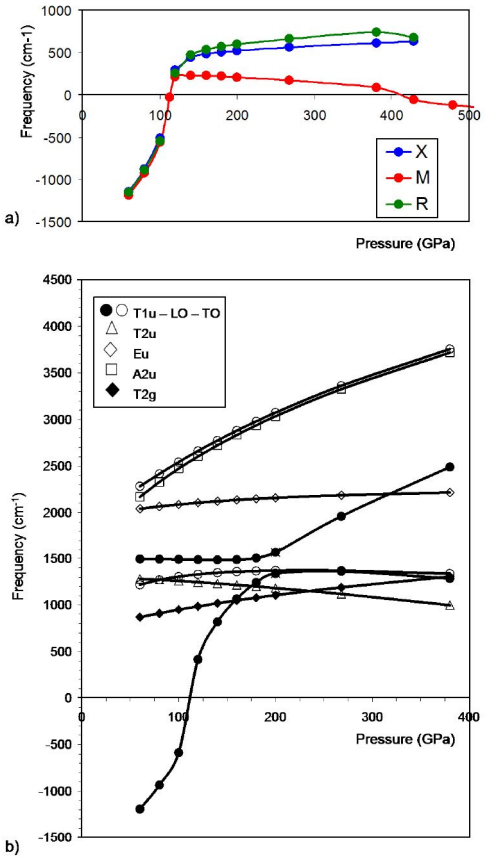

FIG. 2 (color online). Pressure variation of the normal modes in several high-symmetry points. (a) The lowest-frequency modes in ice X in $X = (\frac{1}{2}\ 0\ 0)$, $M = (\frac{1}{2}\ \frac{1}{2}\ 0)$, and $R = (\frac{1}{2}\ \frac{1}{2}\ \frac{1}{2})$. The unstable phonon in M that develops under compression is responsible for the transition to the post-X ice with $Pbcm$ symmetry that was earlier predicted from molecular-dynamics calculations [31]. (b) Pressure variation of the normal modes in Γ in ice X. The lines are guides to the eyes.

ens over only a few GPa: the softening starts at about 120 GPa, and the mode becomes unstable at around 114 GPa [Fig. 2(a)]. Its weakly dispersive character in the reciprocal space denotes a highly localized mode in the direct space: the eigenvectors of this unstable phonon mode in any point of the Brillouin zone correspond to the bouncing back and forth of the hydrogen atoms between the two neighboring oxygen atoms. The movement is done in such a way as at any moment, every O atom has two stronger O-H bonds and two weaker O-H bonds, like in the *ice rule* found at lower pressures [29,30]. This unstable phonon mode is related to the existence of a double-well potential between the two neighboring oxygen atoms. The potential opens at large O-O distances, namely, at low pressure, into a double well, and thus the hydrogen atoms have two energetically equivalent sites as shown in Fig. 3. The depth of the potential increases with increasing O-O distance, i.e., with decreasing pressure. The structure obtained from the freezing-in of this mode is a disordered variant of ice X. This phase has been already confirmed spectroscopically [6,14]. At high pressures, the O-O distances are smaller and the potential closes, such as the hydrogen atoms have only one possible position, hence the resulting symmetry of the hydrogen bond in the ionic phase.

At the other side of the stability field of ice X, at high pressure, one phonon mode softens in the M $(\frac{1}{2}\ \frac{1}{2}\ 0)$ point of the cubic reciprocal space [Fig. 1(c)]. The softening does not appear in other high-symmetry points, like X $(\frac{1}{2}\ 0\ 0)$ and R $(\frac{1}{2}\ \frac{1}{2}\ \frac{1}{2})$ and occurs gradually over a wide pressure range [Fig. 2(a)]. The M point corresponds to a $2 \times 2 \times 1$ supercell that can be reduced to $\sqrt{2} \times \sqrt{2} \times 1$, whose edges are parallel to the diagonals of the cubic basal plane. The unstable phonon consists of displacements parallel to (110) of the atomic planes that contain both oxygen and hydrogen (Fig. 4). The displacements are in antiphase in consecutive planes. It generates a shear of the octahedra that are consequently distorted: they are elongated along

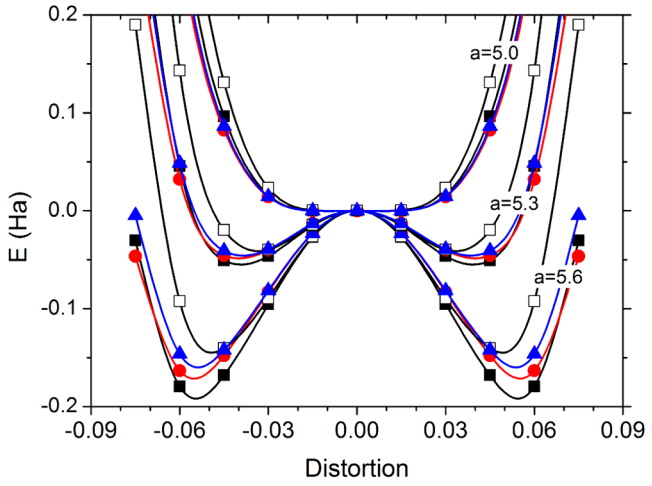

FIG. 3 (color online). The double-well potential corresponding to the soft mode in ice X that develops between any two O neighbors at low pressures. The H atoms can bounce back and forth between the two minima leading to a disordered form of ice X. The potential opens at low pressures (large cells). Solid squares, circles, open squares, and triangles correspond, respectively, to the instability in Γ, X, M, and R. Lattice parameters are in Bohr (1 Bohr = 0.529177 Å).

the former $[\bar{1}10]$ direction of the cubic structure and compressed along the [110] cubic direction. Eventually, there are three types of O-H bonds, four shorter to the equatorial H atoms and one intermediate and one longer to the apical H atoms. The shear imposed to the octahedra contributes to the softening of an acoustic mode [Fig. 1(c)] and yields a better packing of the oxygen sublattice which goes from bcc in ice X to hcp-like in post-X ice.

The space group of the post-X form of ice derived form the phonon instability in M is $Pbcm$. The structure is identical to the one predicted from molecular-dynamics calculations [31]. There are four molecules in the $Pbcm$ structure with O atoms situated in $4d(x\ y\ \frac{1}{4})$, and hydrogen atoms in $4b(\frac{1}{2}\ \frac{1}{2}\ 0)$ and $4c(0\ y\ -\frac{1}{4}\ \frac{1}{4})$. The transition to ice $Pbcm$ was observed around about 350 GPa in molecular-dynamics and is observed slightly above 400 GPa in lattice dynamical calculations. This variation can be due to differences in calculation details, like pseudopotentials or number of plane waves.

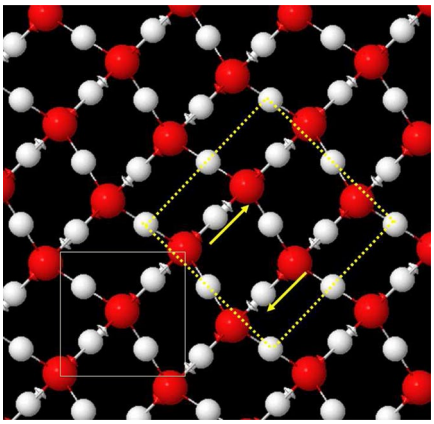

FIG. 4 (color online). The structure of the post-X ice with $Pbcm$ symmetry is obtained by freezing-in the unstable phonon mode in $M(\frac{1}{2}\ \frac{1}{2}\ 0)$ in the cubic structure of ice X at high compression. The $Pbcm$ unit cell (dashed thick line) is in a $\sqrt{2} \times \sqrt{2} \times 1$ relation with the original ice X cell (solid thin line). The $Pbcm$ structure is obtained by alternatingly shifting planes of oxygen and hydrogen parallel to cubic (110).

Our proposed sequence of phase transitions could be easily confirmed experimentally using vibrational spectroscopy. Based on atomic site symmetry and according to group theory, the phonon modes in ice X in Γ decompose as $1\ T_{2g} + 1\ A_{2u} + 1\ E_u + 3\ T_{1u} + 1\ T_{2u}$. The u modes are infrared active, and the T_{2g} mode is the only one visible in Raman [32]. Figure 2(b) shows the pressure variation of the frequency of the normal modes in Γ. At low pressures, the Raman spectra of the disordered ice X is characterized by one broad peak, for example, centered around 870 cm^{-1} at 60 GPa. The disorder weakens and broadens this peak. In the stability field of ice X, all the phonon modes have positive frequencies in the zone center. The Raman spectra have one sharp peak whose intensity decreases by about 40% over the 160–268 GPa pressure range.

The transition to the $Pbcm$ phase is marked by a clear change in both Raman and infrared spectra. The $Pbcm$ phase has 36 modes in Γ that decompose as $5A_u + 6B_{1u} + 7B_{2u} + 6B_{3u} + 4A_g + 4B_{1g} + 2B_{2g} + 2B_{3g}$. The u modes are infrared active except for A_u, and all the g modes are Raman active. Table I lists the LO-TO frequencies of the u-modes for $Pbcm$ ice at 400 GPa, and Fig. 5 shows the Raman spectrum with both peak positions and intensities. The Raman spectra are dominated by the lowest-frequency A_g mode, which corresponds to the former unstable phonon mode from M in ice X that is shear of the octahedra. The second most intense mode corresponds to bending of

TABLE I. u-modes in Γ in ice $Pbcm$ at $\rho = 4.66$ g/cm^3. A_u are silent modes while all the other are infrared active. The modes are computed both in LDA and GGA. Values in parenthesis are in GGA. The density corresponds to 429 GPa in GGA.

	TO	LO		TO	LO
A_u	559(531)		B_{2u}	765(788)	765(788)
	882(949)			1061(1117)	1064(1119)
	1258(1298)			1277(1333)	1448(1358)
	2017(2012)			1833(1857)	1846(1880)
	2628(2560)			2504(2395)	3392(3368)
				3602(3562)	4020(3973)
B_{1u}	990(1052)	996(1064)			
	1309(1358)	1331(1360)	B_{3u}	1061(1135)	1061(1164)
	1377(1406)	1504(1534)		142(1443)	1437(1453)
	2536(2433)	3736(3711)		1776(1795)	1776(1795)
				2193(2218)	2207(2244)
				2432(2346)	3516(3493)
				3875(3828)	3876(3829)

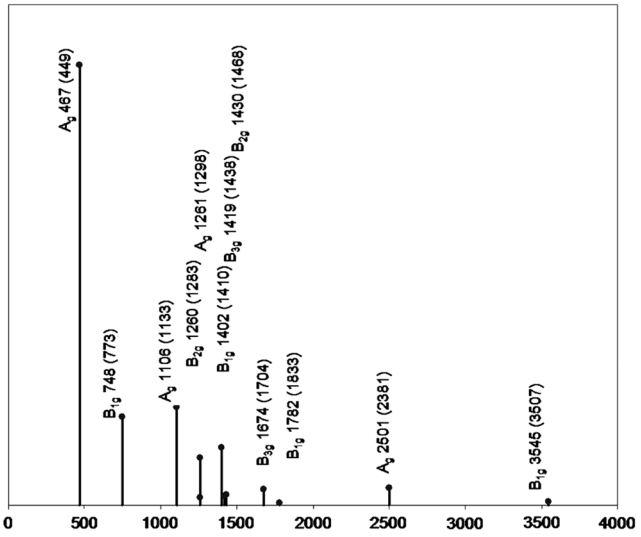

FIG. 5. Raman spectra of ice $Pbcm$ at $\rho = 4.66$ g/cm^3. The intensity of the peaks is computed in LDA and the frequencies both in LDA and GGA. Values in parenthesis are in GGA. The density corresponds to 429 GPa in GGA.

the O-H-O angles, where the H atoms are the apical ones. The modes involving H displacements along the O-H-O bonds are the highest in frequency and have weak Raman response.

Therefore, our work defines the dynamical stability of ice X between about 120 GPa up to about 400 GPa. Based on phonon band dispersion, we show that the phase transition sequence at low temperature and high pressures in ice is ice VIII–disordered ice X–iceX–ice $Pbcm$. The disordered ice X is due to a phonon collapse in the whole Brillouin zone, phonon that corresponds to hydrogen atoms bouncing back and forth between every two oxygen neighbors in a double-well potential. Post-X ice is orthorhombic $Pbcm$ and appears due to a phonon instability in M that distorts the body-centered cubic sublattice of oxygen atoms into a hexagonal closed-packed-like structure. Thus, our calculations also validate the earlier theoretical prediction for a phase transition to a post-X ice structure in H_2O [31].

*razvan.caracas@ens-lyon.fr

[1] D. Fortes, Ph.D. thesis, UCL, University of London 2004 p. 230.
[2] G. P. Johari and O. Andersson, Thermochim. Acta **461**, 14 (2007).
[3] W. B. Holzapfel, J. Chem. Phys. **56**, 712 (1972).
[4] K. S. Schweizer and F. H. Stillinger, J. Chem. Phys. **80**, 1230 (1984).
[5] R. J. Nelmes, J. S. Loveday, W. G. Marshall, G. Hamel, J. M. Besson, and S. Klotz Phys. Rev. Lett. **81**, 2719 (1998).
[6] A. F. Goncharov, V. V. Struzhkin, H.-k. Mao, and R. J. Hemley, Phys. Rev. Lett. **83**, 1998 (1999).
[7] A. Putrino and M. Parrinello, Phys. Rev. Lett. **88**, 176401 (2002).
[8] M. Benoit, A. H. Romero, and D. Marx, Phys. Rev. Lett. **89**, 145501 (2002).
[9] R. J. Hemley, Annu. Rev. Phys. Chem. **51**, 763 (2000).
[10] Ph. Pruzan, J. C. Chervin, E. Wolanin, B. Canny, M. Gauthier, and M. Hanfland, J. Raman Spectrosc. **34**, 591 (2003).
[11] E. Wolanin, Ph. Pruzan, J. C. Chervin, B. Canny, M. Gauthier, D. Hausermann, and M. Hanfland, Phys. Rev. B **56**, 5781 (1997).
[12] K. Aoki, H. Yamawaki, M. Sakashita, and H. Fujihisa, Phys. Rev. B **54**, 15673 (1996).
[13] M. Song, H. Yamawaki, H. Fujihisa, M. Sakashita, and K. Aoki, Phys. Rev. B **60**, 12644 (1999).
[14] A. F. Goncharov, V. V. Struzhkin, M. S. Somayazulu, R. J. Hemley, and H. K. Mao, Science **273**, 218 (1996).
[15] M. Bernasconi, P. L. Silvestrelli, and M. Parrinello, Phys. Rev. Lett. **81**, 1235 (1998).
[16] X. Gonze, J.M. Beuken, R. Caracas, F. Detraux, M. Fuchs, G. M. Rignanese, L. Sindic, M. Verstraete, G. Zerah, F. Jollet, M. Torrent, A. Roy, M. Mikami, P. Ghosez, J. Y. Raty, and D.C. Allan, Comput. Mater. Sci. **25**, 478 (2002).
[17] N. Troullier and J. L. Martins, Phys. Rev. B **43**, 1993 (1991).
[18] H. J. Monkhorst and J. D. Pack, Phys. Rev. B **13**, 5188 (1976).
[19] X. Gonze, Phys. Rev. B **55**, 10337 (1997).
[20] X. Gonze and C. Lee, Phys. Rev. B **55**, 10355 (1997)
[21] S. Baroni, S. de Gironcoli, A. Dal Corso, and P. Giannozzi, Rev. Mod. Phys. **73**, 515 (2001).
[22] X. Gonze, G.-M. Rignanese, and R. Caracas, Z. Kristallogr. **220**, 458 (2005).
[23] M. Veithen, X. Gonze, and P. Ghosez, Phys. Rev. B **71**, 125107 (2005).
[24] G. Placzek, in *Handbuch der Radiologie* (Akademische Verlagsgeselschaft, Leipzig, 1934), Vol. 6, p. 208.
[25] S. A. Prosandeev, U. Waghmare, I. Levin, and J. Maslar, Phys. Rev. B **71**, 214307 (2005).
[26] R. Caracas and R. E. Cohen, Geophys. Res. Lett. doi: **33**, L12S05 (2006).
[27] R. Caracas, J. Chem. Phys. **127**, 144510 (2007).
[28] J. P. Perdew, K. Burke, and M. Ernzerhof, Phys. Rev. Lett. **77**, 3865 (1996).
[29] L. Pauling, J. Am. Chem. Soc. **57**, 2680 (1935).
[30] J. Snyder, J. S. Slusky, R. J. Cava, and P. Schiffer, Nature (London) **413**, 48 (2001).
[31] M. Benoit, M. Bernasconi, P. Focher, and M. Parrinello, Phys. Rev. Lett. **76**, 2934 (1996).
[32] The T_{1g} mode corresponds to oscillations of every oxygen pair around the hydrogen atom in-between, which is left still. The T_{1u} mode corresponds to rotations of the octahedra and the E_{1u} to torsion of the octahedra around the central oxygen atom. The B_{1u} both is the breathing mode of the octahedra. One T_{2u} mode corresponds to bending of the H-O-H angles in opposite directions relative to the central oxygen. The second T_{2u} mode is the bouncing back and forth of the hydrogen atoms between the two neighboring oxygens along O-H-O. The T_{2u} is the unstable mode that is responsible for the transitions to the disordered structure at low pressures.